ChemPubSoc Europe

DOI: 10.1002/cssc.201600843

CHEMSUSCHEM Full Papers

A Nitrogen-Doped Carbon Catalyst for Electrochemical CO_2 Conversion to CO with High Selectivity and Current Density

Huei-Ru Molly Jhong,[a] Claire E. Tornow,[a] Bretislav Smid,[b] Andrew A. Gewirth,[a, b] Stephen M. Lyth,*[b, c] and Paul J. A. Kenis*[a, b]

We report characterization of a non-precious metal-free catalyst for the electrochemical reduction of CO_2 to CO; namely, a pyrolyzed carbon nitride and multiwall carbon nanotube composite. This catalyst exhibits a high selectivity for production of CO over H_2 (approximately 98% CO and 2% H_2), as well as high activity in an electrochemical flow cell. The CO partial current density at intermediate cathode potentials ($V = -1.46$ V vs. Ag/AgCl) is up to 3.5× higher than state-of-the-art Ag nanoparticle-based catalysts, and the maximum current density is 90 mA cm^{-2}. The mass activity and energy efficiency (up to 48%) were also higher than the Ag nanoparticle reference. Moving away from precious metal catalysts without sacrificing activity or selectivity may significantly enhance the prospects of electrochemical CO_2 reduction as an approach to reduce atmospheric CO_2 emissions or as a method for load-leveling in relation to the use of intermittent renewable energy sources.

Introduction

Rising CO_2 levels as a result of human activity have been linked to climate change, leading to, for example, erratic weather patterns and rising ocean temperatures.[1] Multiple approaches should be implemented to curb this increase in CO_2 concentration, including carbon sequestration, electrification of the transportation sector, and switching from using fossil fuels to renewable energy.[2,3] A major challenge in the implementation of wind and solar-derived renewable energy is intermittency, that is, the mismatch between supply and demand. Bridging this gap will require the development of scalable and broadly deployable mass electricity conversion and storage technologies. One interesting method to reduce CO_2 emissions as well as providing a means of mass energy storage, is the electrochemical reduction of CO_2 into useful chemicals, which can then be stored or transported at scale, and used on demand.[4–6] However, catalysts for the electrochemical reduction of CO_2 into products, such as CO, formic acid, methanol, and small hydrocarbons, currently do not exhibit sufficient activity or selectivity for such applications. Metals, such as Ag, and Au, exhibit the best performance for conversion of CO_2 to CO to date.[4,7–9] However, high cost, sensitivity to poisoning, difficulty of reclamation, and insufficient activity hampers their utility and wide-scale adoption.

In the parallel field of fuel cells, high cost, limited durability, and susceptibility of Pt-group electrocatalysts to poisoning have spurred intensive research into alternatives. This includes reducing Pt-loading by using alloys; and the use of non-Pt group metal (non-PGM) catalysts for the oxygen reduction reaction (ORR). Non-PGM electrocatalysts are often variations on N-coordinated Fe or Co in a carbon matrix (i.e., Fe/N/C, Co/N/C), or simply metal-free N-doped carbon.[10,11] N-doped carbon nanotube powders,[12] nanotube arrays,[13] graphene,[14,15] nanocages,[16] and carbon nitrides[17–22] have been studied in recent years for reactions including: (i) the ORR,[17–22] (ii) photocatalytic water splitting,[23,24] and (iii) photocatalytic CO_2 reduction. In (iii), the primary products include CO, methanol, and ethanol, but at low quantum yield.[25,26] We have previously demonstrated that carbon nitride (g-C_3N_4) exhibits ORR activity, especially when synthesized on a conductive support with large surface area.[19–22] High temperature treatment played a critical role in the catalytic activity, with optimal activity achieved after pyrolysis at 1000 °C.[20,21] Such catalysts contain only C and N with trace amounts of dopants/impurities, and are synthesized by simple and scalable methods. Additionally, we have developed organometallic silver heterogeneous catalysts for the CO_2 reduction reaction involving N-containing organic ligands.[27]

The above work led us to the conclusion that such non-PGM N-doped carbon catalysts should be more thoroughly explored

[a] Dr. H.-R. M. Jhong, Dr. C. E. Tornow, Prof. A. A. Gewirth, Prof. P. J. A. Kenis
Department of Chemistry and Chemical & Biomolecular Engineering
University of Illinois at Urbana-Champaign
600 South Mathews Avenue, Urbana, IL 61801 (USA)
E-mail: kenis@illinois.edu

[b] Dr. B. Smid, Prof. A. A. Gewirth, Prof. S. M. Lyth, Prof. P. J. A. Kenis
International Institute for Carbon Neutral Energy Research (WPI-I2CNER)
Kyushu University
Nishi-ku 819-0395, Fukuoka (Japan)
E-mail: lyth@i2cner.kyushu-u.ac.jp

[c] Prof. S. M. Lyth
Energy 2050
Department of Mechanical Engineering
University of Sheffield
S10 2TN (UK)

The ORCID identification number(s) for the author(s) of this article can be found under http://dx.doi.org/10.1002/cssc.201600843.

This publication is part of a Special Issue around the "1st Carbon Dioxide Conversion Catalysis" (CDCC-1) conference. To view the complete issue, visit: http://dx.doi.org/10.1002/cssc.v10.6.

for the electrochemical CO_2 reduction reaction. Relatively few examples of the use of this class of catalyst for CO_2 reduction exist. Kumar et al. reported a N-doped carbon fiber catalyst fabricated by pyrolysis of electrospun mats of polyacrylonitrile (PAN). The micron-scale fibers exhibited some activity for CO_2 reduction to CO, with a current density of up to 5 mA cm^{-2} in a standard three electrode cell.[28] Zhang et al. achieved CO_2 reduction on N-doped carbon nanotubes in aqueous bicarbonate solutions, with a faradaic efficiency of 59%.[29] Recently, Wu et al. achieved a selectivity of 80% and a partial current density for CO formation of 2.25 mA cm^{-2}.[30] Here we explore non-precious metal-free, N-doped carbon catalysts for the electrochemical reduction of CO_2 to CO. This can then be converted into liquid fuels by using, for example, the Fischer–Tropsch process. Specifically, the materials are comprised of carbon nitride (g-C_3N_4) supported on multiwalled carbon nanotubes (MWCNTs), subjected to pyrolysis at 1000 °C to form nitrogen-doped carbon (CN)-coated MWCNT nanocomposites (CN/MWCNT; Figure 1a).

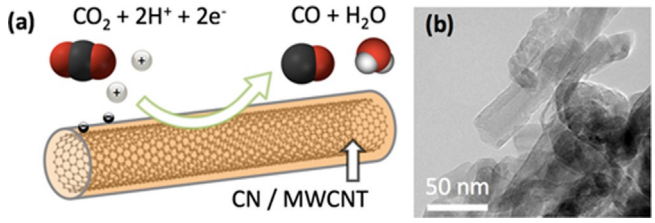

Figure 1. (a) Representation of the electrochemical CO_2 reduction reaction on a CN-coated MWCNT. (b) TEM image of the synthesized CN/MWCNT catalyst powder.

Results and Discussion

Characterization of the CN/MWCNT powder by transmission electron microscopy (TEM) reveals short, defective, and kinked MWCNTs; structural characteristics introduced during the milling step (Figure 1b). The surface area was measured to be 250.2 m^2 g^{-1} by N adsorption. CHN elemental analysis revealed a N content of 0.39 at%. This low N content reflects the fact that the pyrolyzed g-C_3N_4 exists as a thin layer on the surface of the pure MWCNT. The N content of this thin layer is expected to be higher, but the composition of such a thin layer is difficult to determine using conventional characterization techniques. Peaks in the X-ray photoelectron spectroscopy (XPS) survey spectra (Figure 2a) are attributed to C (97.68 at%), N (0.12 at%), and oxygen (2.20 at%). Deconvolution of the N1s peak reveals the probable presence of pyridinic (~398.5 eV, 33.4%), pyrrolic (399.5 eV, 26.3%), tertiary/graphite-like (~400.5 eV, 27.6%), and amine (401.7 eV, 12.7%) N environments (Figure 2b), arising from pyrolysis of the initial g-C_3N_4 coating. Metal impurities (especially Fe) are absent within the detection limits of the machine (Figure 2d); however, trace amounts of the metal may be present as contamination from the stainless steel reaction vessel. The XRD spectrum (Figure 3) is as typically observed for MWCNTs, with sharp peaks corresponding to the (002), (110), and (101) lattice planes of

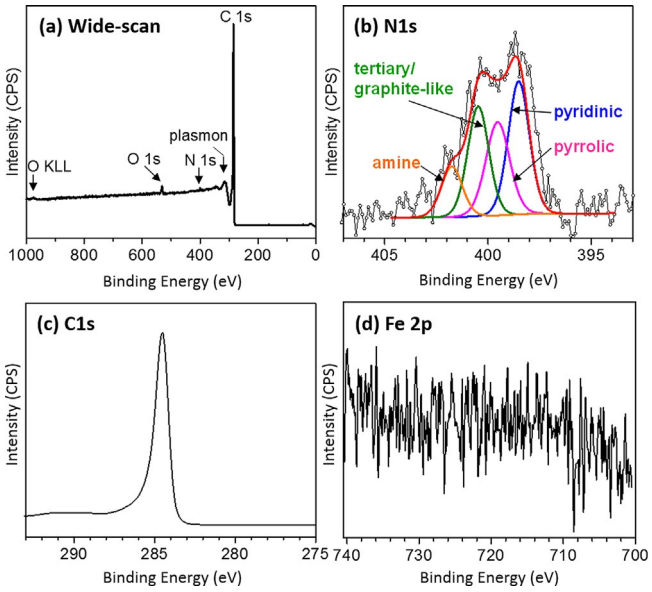

Figure 2. (a) Full XPS survey spectrum of the CN/MWCNT catalyst, and (b) high resolution spectrum of the N1s region. XPS spectrum Fe2p region of the CN/MWCNT sample.

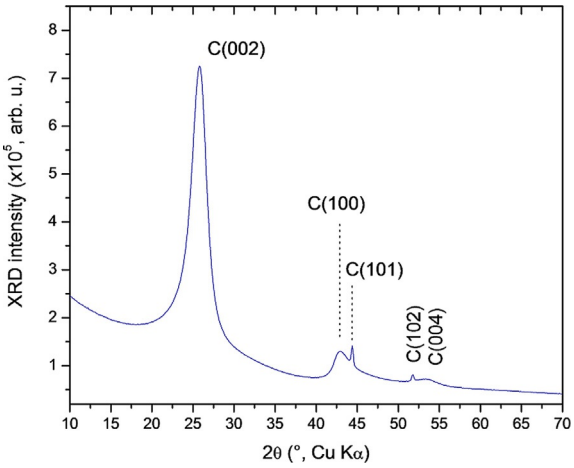

Figure 3. XRD spectrum of the CN/MWCNT catalyst.

carbon. The N-doped carbon coating is expected to have broad, low intensity peaks at around 25° and 44° reflecting low crystallinity.[15] However, these are masked by the intense MWCNT signal, reflecting the relatively thin nature of the N-doped carbon coating.

The activity of the CN/MWCNT catalyst for electroreduction of CO_2 was determined and compared with a state-of-the-art Ag nanoparticle catalyst. Cyclic voltammetry (CV) was performed in a three electrode cell. CN/MWCNT exhibits around five times higher activity for CO_2 conversion compared to the Ag nanoparticles, although the Ag catalyst displays an earlier onset potential (Figure 4). This result suggests promise for application of the CN/MWCNT in CO_2 electrolysis, especially at high current densities.

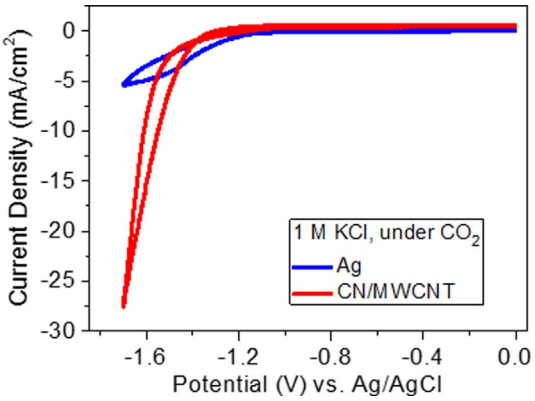

Figure 4. Cyclic voltammetry measuring the CO_2 reduction activity of the CN/MWCNT and Ag catalysts in a standard three electrode electrochemical cell (1 M KCl, 25 mV s^{-1}).

Subsequently, the CO_2 reduction activity was tested using a CO_2 electrolysis cell.[7] The cathode electrocatalyst was sprayed onto a carbon paper gas diffusion electrode (GDE) and assembled into the cell. Analysis via X-ray micro-computed tomography (MicroCT) revealed a uniform and crack-free electrocatalyst layer (Figure 4a) supported on the highly porous GDE. Cross-sectional observation using scanning electron microscopy (SEM) confirms that the CN/MWCNT catalyst layer uniformly coats the GDE with a thickness of around 15 μm (Figure 5b). Higher magnification SEM images of the CN/MWCNT electrocatalyst layer reveal agglomerates of varying sizes at the micron-scale (Figure 5c). This microstructure may improve the accessible surface area and enhance mass diffusion through the electrocatalyst layer.

Figure 6 shows the performance of the microfluidic CO_2 electrolysis cell operated with the CN/MWCNT catalyst, and compared with Ag nanoparticles. The anode reaction is Cl_2 evolution, given that the electrolyte used is 1 M KCl. Only H_2 and CO were detected as products at the cathode, and the following are likely reaction mechanisms [Eq. (1)–(2)]:

$$2\,H^+ + 2\,e^- + CO_2 \rightarrow H_2O + CO \quad (1)$$

$$2\,H^+ + 2\,e^- \rightarrow H_2 \quad (2)$$

The CN/MWCNT cathode catalyst displays significantly higher CO partial current density than the Ag catalyst at cathode potentials of −1.2 to −1.6 V vs. Ag/AgCl, revealing that the CN/MWCNT catalyst is highly active for the conversion of CO_2 to CO (Figure 6a). The cell produces a partial CO current density of up to 90 mA cm^{-2} at a cathode potential of −1.62 V vs. Ag/AgCl, when operated with the CN/MWCNT cathode catalyst. These values are much higher than those previously reported in the literature for other N-doped carbon systems.[28–30] The performance was stable at least over a period of several hours. Furthermore, the CO partial current density for CN/MWCNT is up to 3.5× higher than the state-of-the-art Ag nanoparticle-based catalyst at intermediate cathode potential ($V = -1.46$ V vs. Ag/AgCl). The mass activity (i.e., normalized to catalyst loading) gives a clearer comparison between the two catalysts. In this case, at −1.46 V vs. Ag/AgCl, the mass activity of CN/MWCNT is 29.2 A g^{-1}, compared with 26.7 A g^{-1} for the Ag nanoparticles. This indicates that the non-precious catalysts actually have comparable mass activity to the current state-of-the-art at this intermediate cathode potential.

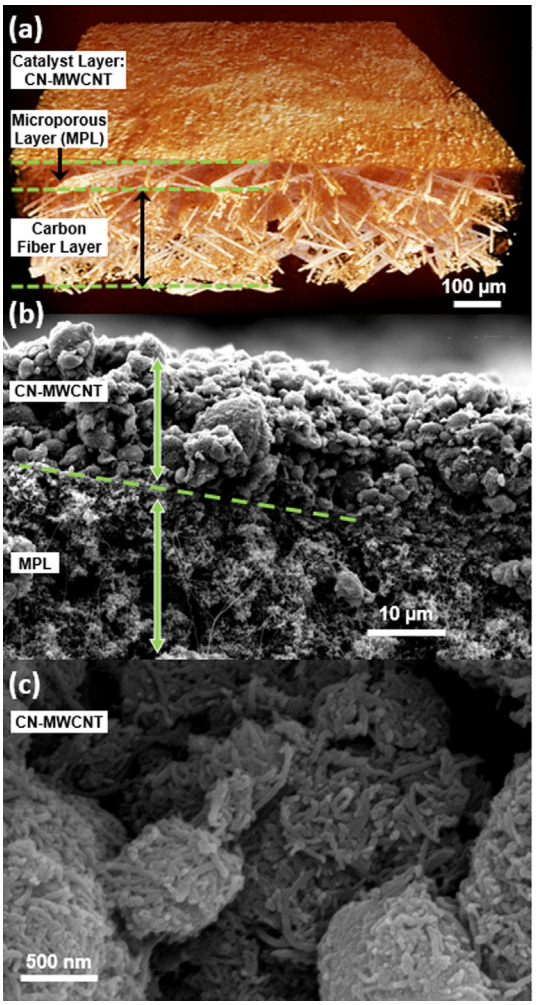

Figure 5. (a) Reconstructed 3D view of the electrode obtained from MicroCT data. (b) SEM cross-sectional image of the CN/MWCNT catalyst layer on the microporous layer of the gas diffusion electrode. (c) SEM images of the CN/MWCNT electrocatalyst layer (loading 2.39 mg cm^{-2}).

The CN/MWCNT catalyst also catalyzes H_2 formation to a small extent, whereas the Ag cathode produces nearly no H_2 within the detection limit of the gas chromatograph. Figure 5b indicates that CN/MWCNT exhibits excellent selectivity for CO over H_2 (i.e., 98% CO and 2% H_2). Again, this is much higher than values previously reported in the literature.[28–30] The overall energetic efficiency is the fraction of energy supplied to the reactor that is successfully transferred to chemical bonds in the desired product. Here, values of 48% and 44% are obtained for the CN/MWCNT cathode catalyst at −1.46 V vs. Ag/AgCl (−2.75 V cell potential) and −1.62 V vs. Ag/AgCl (−3.0 V cell potential), respectively. In comparison, the Ag catalyst exhibits an energetic efficiency of just 42% at a cathode potential of −1.68 V vs. Ag/AgCl (−3.0 V cell potential). The slightly

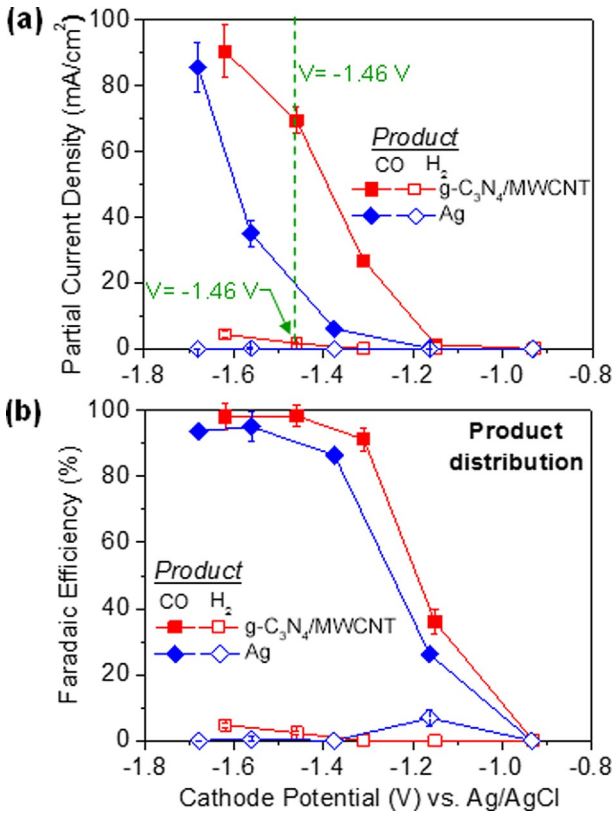

Figure 6. Electrochemical characterization of the CN/MWCNT and Ag catalysts: (a) Partial current densities versus cathode potential for CO and H_2; (b) Faradaic efficiency versus cathode potential for CO and H_2. The error bars represent the standard deviation of the average of three experiments each with freshly prepared working electrodes ($N=3$). Cathode catalyst: 2.39 mg cm^{-2} CN/MWCNT or 0.75 mg cm^{-2} unsupported Ag nanoparticles. Anode catalyst: 4.25 mg cm^{-2} unsupported Pt black. Reactant streams: 7 sccm CO_2; 1.0 M KCl electrolyte flowing at 0.5 mL min^{-1}. Data was collected at room temperature and at ambient pressure.

higher energy efficiency observed for CN/MWCNT can be attributed to the better selectivity for CO over H_2 (Figure 6b). In short, the CN/MWCNT catalyst exhibits high activity, selectivity, and efficiency for the electrochemical reduction of CO_2 to CO, with better performance than other catalysts reported to date, including state-of-the-art Ag nanoparticle catalysts.[7]

The origin of electrochemical CO_2 reduction activity in N-doped carbons was recently investigated by comprehensive density functional theory calculations.[30,31] These revealed that N incorporation modifies the electronic properties of carbon, resulting in a reduced energy barrier for the formation of a COOH intermediate (the rate-limiting step). N doping also results in strong adsorption of the COOH intermediate, and weak adsorption of the CO or HCOOH products. However, in these studies, the highest catalytic activity was exhibited by pyrrolic N sites, leading exclusively to HCOOH as the product.[30] This is in contrast to the experimental results reported here in which a mixture of different N types was detected, and no formic acid was detected in the product stream. This suggests that more work needs to be done to reconcile experiment and theory. This will be the subject of future work.

Conclusions

We report a non-precious N-doped carbon catalyst for the electrochemical reduction of CO_2 to CO in an electrochemical flow cell. This exhibits low onset potential, and high current density, selectivity, as well as energetic efficiency, outperforming results obtained in the existing literature for other N-doped carbon systems. Despite the early stage of development, this catalyst already outperforms state-of-the-art Ag nanoparticle catalysts. Moving away from precious metal catalysts without sacrificing activity or selectivity offers hope for electrochemical CO_2 reduction to become an economically viable process, by largely reducing the capital cost. Further experimental and computational efforts are required to better understand the catalytic mechanism, and to further optimize the cell performance.

Experimental Section

Preparation of the CN/MWCNT catalyst (Scheme 1). Cyanuric chloride (1,3,5-trichlorotriazine, $C_3N_3Cl_3$), sodium azide (NaN_3), benzene, and MWCNTs (cheaptubes.com) were added to a magnetically

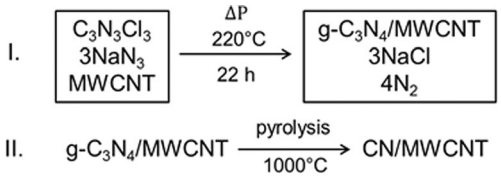

Scheme 1. Synthesis of the CN/MWCNT catalyst.

stirred, stainless-steel high pressure reactor. All materials were used as-received without further purification. The reactor was heated to 220 °C for 22 h, and the $C_3N_3Cl_3$ and NaN_3 reacted to yield MWCNTs coated with g-C_3N_4,[32–34] according to Equation (3):[21]

$$C_3N_3Cl_3 + 3\,NaN_3 \rightarrow g\text{-}C_3N_4 + 3\,NaCl + 4\,N_2 \quad (3)$$

The products were removed from the reactor, washed with benzene and Millipore water, and then heated overnight at 80 °C under vacuum. Subsequently the material was milled in silicon carbide pots, and then subject to pyrolysis at 1000 °C in flowing N_2 to form CN/MWCNT. Surface area was performed by Brunauer–Emmett–Teller (BET) nitrogen adsorption analysis (Belsorp mini II-VS, Bel Japan, Inc.).

Preparation of the Ag nanoparticle catalyst. Ag nanoparticles were purchased from Sigma–Aldrich (nominal size, <100 nm). The actual average particle size was measured as 70 nm by dynamic light scattering, and confirmed by TEM.[35]

Transmission electron microscopy. TEM was used to determine the morphology of the CN/MWCNT catalyst (JEOL, JEM2010), operated at 200 kV. The CN/MWCNT powder was suspended in isopropyl alcohol (Sigma–Aldrich) and sonicated for 30 min to ensure good catalyst dispersion. TEM grids were prepared by dropping the dilute suspension onto copper grids, which were then dried overnight.

Elemental analysis. A CHN elemental analyzer (Yanaco, CHN corder MT-6) was used to determine the N content of the CN/MWCNT sample. XPS was carried out to characterize the chemical composition and N types in the carbon matrix of CN/MWCNT. XPS spectra were collected using a Kratos Axis ULTRA X-ray photoelectron spectrometer with monochromatic Al K-alpha excitation, 120 W (120 kV, 10 mA). Data were collected using a hybrid lens setting with a slot aperture of 300×700 mm^2 analytical area. Charge neutralizer settings of 2.1 A filament current, 2.1 V charge balance and 2 V filament bias were used. Survey spectra were collected at a pass energy of 160 eV and high resolution spectra were collected using a pass energy of 40 eV. The data were fitted to Gaussian–Lorentzian curves. The binding energy was referenced to the graphitic C1 s line at 284.5 eV.

Preparation of Electrodes. Previously we reported the preparation of GDEs for use in a CO_2 electrolysis cell.[7] Sigracet 35 BC gas diffusion layers (GDLs, Ion Power) were used, which consist of 5 wt% poly-tetrafluoroethylene (PTFE)-treated carbon paper that has a teflonized microporous layer on one side. Here the cathodes were air-brushed, whereas the anode was hand-painted using previously described methods.[7] For the Ag cathodes, catalyst inks were prepared by mixing 2.42 mg Ag, 1.85 μL Nafion solution, 200 μL Millipore water, and 200 μL isopropyl alcohol. For the CN/MWCNT cathodes, catalyst inks were prepared by mixing 6.95 mg CN/MWCNT catalyst, 5.33 μL Nafion solution, 200 μL Millipore water, and 200 μL isopropyl alcohol. For the hand-painted anodes, catalyst inks were prepared by mixing 10 mg Pt black (Alfa Aesar), 6.9 μL Nafion solution, 400 μL of Millipore water, and 400 μL isopropyl alcohol. The catalyst loading of the GDEs was determined by weighing the GDE before and after deposition. The Ag cathodes were coated with 0.75 $mg_{Ag}\,cm^{-2}$ and the CN/MWCNT cathodes were covered with 2.39 $mg_{CN/MWCNT}cm^{-2}$. The same anode was used for all measurements, with a catalyst loading of 4.25 mg cm^{-2} Pt black. All inks were sonicated for 20 min to ensure uniform mixing and were either hand-painted using a paintbrush or air-brushed using an automated air-brushing deposition setup onto the teflonized carbon side of the GDL to create a GDE covered with catalyst over a geometric area of 2 cm^2.

Scanning electron microscopy. The morphology of the CN/MWCNT catalyst particles within the catalyst layer of the GDE was characterized using SEM (Philips XL30 ESEM-FEG). For cross-sectional images the GDE was broken using liquid N_2 cracking using a razor blade and the images were acquired using an acceleration voltage of 7.5 kV, a spot size of 3.0 nm, and a working distance of 10.7 mm. Top-down images were acquired using an acceleration voltage of 7.5 kV, a spot size of 2.0 mm, and a working distance of 7.5 mm.

Micro-computed X-ray tomography. We used the same acquisition and reconstruction procedures as reported in our prior work.[36] In short, the whole GDE was clamped in a rotating sample holder and a corner was exposed to the X-ray beam field. During MicroCT imaging (Micro-XCT 400, Xradia), the sample was scanned using an X-ray source at 40 kV and 200 μA, and 745 projections were collected as the sample was rotated stepwise over 180° with a 10 s exposure time for each projection. The projection images were then processed to reconstruct 2D radiographic cross-sectional image stacks and 3D tomographic virtual models of the GDE. The initial reconstruction of MicroCT data was conducted using the TXM Reconstructor reconstruction software (Xradia), which accompanies the MicroCT hardware. The distances of the sample to the X-ray source (76 mm) and the X-ray detector (28 mm) resulted in a voxel (volume pixel) size of 1 μm^3. The field of view (FOV) was approximately 1000×1000 μm.

Electrochemical flow cell measurements. Two catalyst-coated GDEs, an anode and a cathode, were placed on opposite sides of a 0.15 cm-thick poly(methyl methacrylate) (PMMA) sheet with a 0.5 cm wide by 2.0 cm long window (1 cm^2) such that the catalyst layers faced the flowing liquid electrolyte. The geometric surface area used to calculate current density was 1 cm^2. This three-layer assembly was clamped between two Al current collectors with access windows. On the cathode side an Al gas flow chamber supplied CO_2 while the anode was open to the atmosphere so formed O_2 can escape. The assembly was held together with four bolts with Teflon washers to maintain electric isolation between electrodes. CO_2 electrolysis experiments were conducted using a potentiostat (Autolab PG30) at room temperature and ambient pressure. CO_2 gas (S. J. Smith, 100%) was fed at a rate of 7 sccm. In all experiments, the electrolyte flow rate was 0.5 mL min^{-1} controlled by a syringe pump (Harvard Appartus PhD 2000). The electrolyte was 1 M potassium chloride (KCl, Sigma–Aldirch, >99.9995% pure) in water. Millipore water was used for all electrolytes. Electrolysis cell polarization curves were obtained by steady-state chronoamperometric measurements in which gaseous products, as well as unreacted CO_2, were collected and injected into a gas chromatograph (Trace GC, ThermoFisher Scientific) equipped with a thermal conductivity detector for quantitative determination of product composition. Individual anode and cathode polarization curves were independently measured using an external Ag/AgCl reference electrode, which was ionically connected to the electrolyzer.

Electrochemical data analysis. The Faradaic efficiency (FE_k) of a gaseous product k was calculated using Equation (4):

$$FE_k = \frac{n_k F x_k F_m}{I}$$

Where n_k is the number of electrons exchanged ($n_k=2$ for reduction of CO_2 to CO), F is Faraday's constant ($F=96485$ C mol^{-1}), x_k is the mole fraction of the gaseous product k in the gaseous mixture (also equal to the volume fraction if gases are assumed to be ideal), F_m is the molar flow rate (mol s^{-1}), and I is the total current (A). Specifically, we calculated x_k and F_m using Equations (5) and (6):

$$x_k = \frac{F_{v,CO}}{F_{v,CO}+F_{v,CO_2}} = \frac{F_{v,CO}/F_{v,CO_2}}{1+F_{v,CO}/F_{v,CO_2}}$$

$$F_m = \frac{PF_v}{RT}$$

Where $F_{v,CO}$ and F_{v,CO_2} are the volumetric flow rates (cm^3 s^{-1}) of CO and CO_2, respectively. P is the atmospheric pressure ($P=1$ atm), R the gas constant ($R=82.06$ cm^3 atm K^{-1} mol^{-1}), and T the temperature ($T=293$ K). The energetic efficiency (EE_k) for the gaseous product k was calculated using Equation (7):

$$EE_k(\%) = \frac{E^\circ}{V_{cell}} \times FE_k(\%)$$

Where E° is the equilibrium cell potential ($E^\circ = E^\circ_{cathode} - E^\circ_{anode} = -0.10\,V - 1.23\,V = -1.33\,V$ for CO_2 reduction to CO and $E^\circ = E^\circ_{cathode} - E^\circ_{anode} = 0\,V - 1.23\,V = -1.23\,V$ for H_2 evolution), V_{cell} is the applied cell potential, and FE_k is the Faradaic efficiency of the gaseous product k. The overall cell energetic efficiency is the sum of the energetic efficiencies for CO and H_2.

Acknowledgements

We gratefully acknowledge financial support from the Department of Energy (DE-FG02005ER46260), the Department of Energy through an STTR grant to Dioxide Materials and UIUC (DE-SC0004453), and the National Science Foundation (CTS 05-47617). The International Institute of Carbon Neutral Energy Research (WPI-I2CNER), sponsored by the World Premier International Research Center Initiative (WPI), MEXT, Japan. The authors are grateful for support from the Progress 100 program of Kyushu University, supported by MEXT, Japan. We also acknowledge Yohan Kim for assistance in electrochemical testing, Richard Haasch, from the Frederick Seitz Materials Research Laboratory Central Facilities for assistance with XPS, Scott Robinson from the Beckman Institute for assistance with SEM imaging, and Steven R Caliari, Sumit Verma, and Byoungsu Kim for stimulating discussions.

Keywords: catalysis · carbon nanotubes · carbon nitride · co2 conversion · metal-free

[1] S. J. Davis, K. Caldeira, H. D. Matthews, *Science* **2010**, *329*, 1330.
[2] S. Pacala, R. Socolow, *Science* **2004**, *305*, 968.
[3] S. J. Davis, L. Cao, K. Caldeira, M. I. Hoffert, *Environ. Res. Lett.* **2013**, *8*, 011001.
[4] H. R. Jhong, S. Ma, P. J. A. Kenis, *Curr. Opin. Chem. Eng.* **2013**, *2*, 191.
[5] A. M. Appel, J. E. Bercaw, A. B. Bocarsly, H. Dobbek, D. L. DuBois, M. Dupuis, J. G. Ferry, E. Fujita, R. Hille, P. J. A. Kenis, C. A. Kerfeld, R. H. Morris, C. H. F. Peden, A. R. Portis, S. W. Ragsdale, T. B. Rauchfuss, J. N. H. Reek, L. C. Seefeldt, R. K. Thauer, G. L. Waldrop, *Chem. Rev.* **2013**, *113*, 6621.
[6] D. T. Whipple, P. J. A. Kenis, *J. Phys. Chem. Lett.* **2010**, *1*, 3451.
[7] H. R. Jhong, F. R. Brushett, P. J. A. Kenis, *Adv. Energy Mater.* **2013**, *3*, 589.
[8] Y. H. Chen, C. W. Li, M. W. Kanan, *J. Am. Chem. Soc.* **2012**, *134*, 19969.
[9] W. L. Zhu, R. Michalsky, O. Metin, H. F. Lv, S. J. Guo, C. J. Wright, X. L. Sun, A. A. Peterson, S. H. Sun, *J. Am. Chem. Soc.* **2013**, *135*, 16833.
[10] H. A. Gasteiger, N. M. Markovic, *Science* **2009**, *324*, 48.
[11] J. Liu, S. Yu, T. Daio, M. S. Ismail, K. Sasaki, S. M. Lyth, *J. Electrochem. Soc.* **2016**, *163*, F1049.
[12] T. Sharifi, G. Hu, X. E. Jia, T. Wagberg, *ACS Nano* **2012**, *6*, 8904.
[13] K. Gong, F. Du, Z. Xia, M. Durstock, L. Dai, *Science* **2009**, *323*, 760.
[14] Z. Q. Luo, S. H. Lim, Z. Q. Tian, J. Z. Shang, L. F. Lai, B. MacDonald, C. Fu, Z. X. Shen, T. Yu, J. Y. Lin, *J. Mater. Chem.* **2011**, *21*, 8038.
[15] J. Liu, D. Takeshi, D. Orejon, K. Sasaki, S. M. Lyth, *J. Electrochem. Soc.* **2014**, *161*, F544.
[16] S. Chen, J. Y. Bi, Y. Zhao, L. J. Yang, C. Zhang, Y. W. Ma, Q. Wu, X. Z. Wang, Z. Hu, *Adv. Mater.* **2012**, *24*, 5593.
[17] Y. Zheng, Y. Jiao, J. Chen, J. Liu, J. Liang, A. Du, W. Zhang, Z. Zhu, S. C. Smith, M. Jaroniec, G. Q. M. Lu, S. Z. Qiao, *J. Am. Chem. Soc.* **2011**, *133*, 20116.
[18] Y. Q. Sun, C. Li, Y. X. Xu, H. Bai, Z. Y. Yao, G. Q. Shi, *Chem. Commun.* **2010**, *46*, 4740.
[19] S. M. Lyth, Y. Nabae, S. Moriya, S. Kuroki, M. Kakimoto, J. Ozaki, S. Miyata, *J. Phys. Chem. C* **2009**, *113*, 20148.
[20] S. M. Lyth, Y. Nabae, N. M. Islam, S. Kuroki, M. Kakimoto, S. Miyata, *J. Electrochem. Soc.* **2011**, *158*, B194.
[21] S. M. Lyth, Y. Nabae, N. M. Islam, S. Kuroki, M. Kakimoto, S. Miyata, *J. Nanosci. Nanotechnol.* **2012**, *12*, 4887.
[22] S. M. Lyth, Y. Nabae, N. M. Islam, T. Hayakawa, S. Kuroki, M. Kakimoto, S. Miyata, N. Md, I. Teruaki, *e-J. Surf. Sci. Nanotechnol.* **2012**, *10*, 29 – 32.
[23] X. C. Wang, K. Maeda, A. Thomas, K. Takanabe, G. Xin, J. M. Carlsson, K. Domen, M. Antonietti, *Nat. Mater.* **2009**, *8*, 76.
[24] K. Maeda, X. C. Wang, Y. Nishihara, D. L. Lu, M. Antonietti, K. Domen, *J. Phys. Chem. C* **2009**, *113*, 4940.
[25] G. H. Dong, L. Z. Zhang, *J. Mater. Chem.* **2012**, *22*, 1160.
[26] J. Mao, T. Y. Peng, X. Zhang, K. Li, L. Ye, L. Zan, *Catal. Sci. Technol.* **2013**, *3*, 1253.
[27] C. E. Tornow, M. R. Thorson, S. Ma, A. A. Gewirth, P. J. A. Kenis, *J. Am. Chem. Soc.* **2012**, *134*, 19520.
[28] B. Kumar, M. Asadi, D. Pisasale, S. Sinha-Ray, B. A. Rosen, R. Haasch, J. Abiade, A. Yarin, A. Salehi-Khojin, *Nat. Commun.* **2013**, *4*, 2819.
[29] S. Zhang, P. Kang, S. Ubnoske, M. K. Brennaman, N. Song, R. L. House, J. T. Glass, T. J. Meyer, *J. Am. Chem. Soc.* **2014**, *136*, 7845.
[30] J. Wu, R. M. Yadav, M. Liu, P. P. Sharma, C. S. Tiwary, L. Ma, X. Zou, X.-D. Zhou, B. I. Yakobson, J. Lou, P. M. Ajayan, *ACS Nano* **2015**, *9*, 5364.
[31] Y. Liu, J. Zhao, Q. Cai, *Phys. Chem. Chem. Phys.* **2016**, 18, 5491 – 5498.
[32] Y. Zheng, J. Liu, J. Liang, M. Jaroniec, S. Z. Qiao, *Energy Environ. Sci.* **2012**, *5*, 6717.
[33] Y. Wang, X. C. Wang, M. Antonietti, *Angew. Chem. Int. Ed.* **2012**, *51*, 68; *Angew. Chem.* **2012**, *124*, 70.
[34] A. Thomas, A. Fischer, F. Goettmann, M. Antonietti, J.-O. Müller, R. Schlögl, J. M. Carlsson, *J. Mater. Chem.* **2008**, *18*, 4893.
[35] A. Salehi-Khojin, H.-R. M. Jhong, B. A. Rosen, W. Zhu, S. Ma, P. J. A. Kenis, R. I. Masel, *J. Phys. Chem. C* **2013**, *117*, 1627.
[36] H.-R. Jhong, F. R. Brushett, L. Yin, D. M. Stevenson, P. J. A. Kenis, *J. Electrochem. Soc.* **2012**, *159*, B292.

Received: June 24, 2016
Revised: September 23, 2016
Published online on October 28, 2016